Supplementary Information

Heterometal-organic frameworks as highly sensitive and highly selective luminescent probes to detect I^- ions in aqueous solutions

Peng-Fei Shi[ab], Huan-Cheng Hu[a], Zhan-Yun Zhang[a], Gang Xiong[a] and Bin Zhao*[a]

[a] Department of Chemistry, Key Laboratory of Advanced Energy Material Chemistry, MOE, and Collaborative Innovation Center of Chemical Science and Engineering (Tianjin), Nankai University, Tianjin 300071, P. R. China

[b] School of Chemistry and Chemical Engineering, Linyi University, Linyi 276005, P. R. China

Experimental Section

(1) Synthesis of **1**·$\mathbf{NO_3^-}$ and **2**·$\mathbf{NO_3^-}$.

A mixture of H_2L (0.0488 g, 0.2 mmol), $Zn(NO_3)_2·6H_2O$ (0.0148 g, 0.05 mmol), 0.1 mmol $Ln(NO_3)_3·6H_2O$ (0.0446 g, $Eu(NO_3)_3·6H_2O$; 0.0453 g, $Tb(NO_3)_3·6H_2O$), 4 mL distilled water and 4 mL anhydrous alcohol were sealed in a Teflon-lined stainless vessel (25 mL) and heated at 160 ℃ for 48 h under autogenous pressure. The vessel was then cooled slowly down to the room temperature at 5 ℃/ h. Colorless needlelike crystals were obtained. The yield was 72% for **1**·$\mathbf{NO_3^-}$ and 83 % for **2**·$\mathbf{NO_3^-}$ (based on $Ln(NO_3)_3·6H_2O$). Elemental anal (%):Calcd: C, 28.41; H, 3.31; N: 7.36 Found: C, 28.64; H, 3.45; N: 7.05 for **2**·$\mathbf{NO_3^-}$; Calcd: C, 28.67; H, 3.34; N: 7.43 Found: C, 28.39; H, 3.09; N: 7.75 for **1**·$\mathbf{NO_3^-}$. CCDC Number: 969413 for **1**·$\mathbf{NO_3^-}$, 969414 for **2**·$\mathbf{NO_3^-}$.

(2) Preparation of **1**·$\mathbf{I^-}$, **2**·$\mathbf{I^-}$ and **2**·$\mathbf{Br^-}$

Single crystals of **1**·$\mathbf{I^-}$, **2**·$\mathbf{I^-}$ and **2**·$\mathbf{Br^-}$ were obtained from single-crystal to single-crystal transformation when 50 mg single crystals of **1**·$\mathbf{NO_3^-}$ or **2**·$\mathbf{NO_3^-}$ were immersed in a 5 mL solution of 5 equiv KI (KBr) for 12 h, respectively. CCDC Number: 986347 for **2**·$\mathbf{Br^-}$, 986348 for **2**·$\mathbf{I^-}$.

(3) Luminescence response to different common anions

50 mg **1**·$\mathbf{NO_3^-}$ or **2**·$\mathbf{NO_3^-}$ was placed into 50 mL distilled H_2O and ultrasonic agitated for 30 min, resulting in the aqueous suspension. Then 50 μL of 1×10^{-3} mol·L^{-1} common inorganic salt aqueous solution of NaN_3 or K_mX solution (m = 1, X = F, Cl, Br, I, CH_3COO, NO_3, H_2PO_4, HSO_3, HCO_3, SCN^-; m = 2, X = CO_3, SO_4, SO_3; m = 3, X = PO_4) was respectively added to 950 μL suspension prepared above. After 10 s, the luminescence of the solution was measured respectively.

(4) Selectively to detect I^-

13 common inorganic salt aqueous solution of K_mX with the concentration of 1×10^{-3} mol·L^{-1} (m = 1, X= F, Cl, CH_3COO, NO_3, H_2PO_4, HSO_3, HCO_3; m = 2, X = CO_3, SO_4, SO_3; m = 3, X = PO_4) were prepared, and each kind of solution was taken out 10 μL and added together to the 870 μL aqueous suspensions of **1**·$\mathbf{NO_3^-}$ or **2**·$\mathbf{NO_3^-}$ to form **1**·**X** and **2**·**X**, respectively. After 10 s, the luminescence of the mixed solution **1**·**X** and **2**·**X** were measured. Then, 10 μL 1×10^{-3} mol·L^{-1} KI was respectively added to the mixed solution **1**·**X** or **2**·**X**. After 10 s, the luminescence was measured respectively.

(5) Luminescence response to I^- with different concentrations

5×10^{-7}~1×10^{-3} mol·L^{-1} KI was respectively added to the aqueous suspension of **1**·$\mathbf{NO_3^-}$. Then, the luminescence was measured respectively; 1×10^{-8}~1×10^{-4} mol·L^{-1} KI was respectively added to the aqueous suspension of **2**·$\mathbf{NO_3^-}$. Then, the luminescence was measured, respectively.

(6) Regeneration of **2**·$\mathbf{NO_3^-}$

2·$\mathbf{I^-}$ was immersed in KNO_3 (with the KNO_3/**2**·$\mathbf{I^-}$) molar ratio of 10/1) aqueous solution for 3 h respectively. Then, the samples were washed by distilled H_2O for several times and collected.

(7) Anion exchange with I^-

50 mg sample of **1**·$\mathbf{NO_3^-}$ or **2**·$\mathbf{NO_3^-}$ was immersed in a 5 mL solution of 5 equiv KI. Every ten minutes, the solution was centrifuged, separated from the solid sample and monitored by UV spectrophotometer respectively. After each test, the solution was poured back into the beaker for further anion exchange.

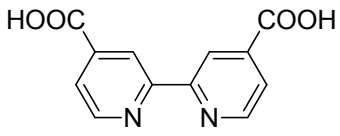

Scheme S1. The structure of H_2L.

Instrumental Details

Elemental analyses for C, H, and N were obtained at the Institute of Elemental Organic Chemistry, Nankai University. Thermogravimetric analyses (TGA)

experiments were performed on a NETZSCH TG 209 instrument with a heating rate of $10^0 C min^{-1}$. Powder X-ray diffraction measurements were recorded on a D/Max-2500 X-ray diffractometer using Cu-Kα radiation. Energy Dispersive Spectrometer (EDS) tests were measured on field emission scanning electron microscopy (SEM, JEOLJSM7500F). UV-Vis spectroscopic studies were collected on a HITACHI U-3900 and JASCO V-570 spectrophotometer. X-ray photoelectron spectroscopy (XPS) tests were performed on Kratos Axis Ultra DLD multi-technique. Raman spectrum was measured on Bruker RFS100/S. The Luminescent spectra were measured on a HITACHI F-4600 FL spectrophotometer.

X-ray Crystallography

Crystallographic data of **1**·$\mathbf{NO_3^-}$, **2**·$\mathbf{NO_3^-}$ and **2**·$\mathbf{I^-}$ were collected on a SuperNova Single Crystal Diffractometer equipped with graphite-monochromatic MoKα radiation (λ = 0.71073 Å). The data integration and empirical absorption corrections were carried out by SAINT programs. The structures are solved by direct methods (SHELXS 97). All the non-hydrogen atoms are refined anisotropically on F^2 by full-matrix least-squares techniques (SHELXL 97). All the hydrogen atoms except for those of the uncoordinated water molecules in these coordination polymers are generated geometrically and refined isotropically using the riding model. Additionally, NO_3^- in **1**·$\mathbf{NO_3^-}$ and **2**·$\mathbf{NO_3^-}$ are disordered, which are refined with a disordered model and some N-O bonds are restrained.

Crystal structures of **2**·$\mathbf{I^-}$

Crystallographic details of it are summarized in Table S1. As shown in Fig. S1, the cationic frameworks of **2**·$\mathbf{I^-}$ still remain the same as that in **2**·$\mathbf{NO_3^-}$. Interestingly, I^- ions exchange with NO_3^-, and I_3^- reside in the channels of **2**·$\mathbf{I^-}$ with typical I-I bonds 3.04 and 2.58 Å, which fall into the normal range of I-I bond lengths[1].

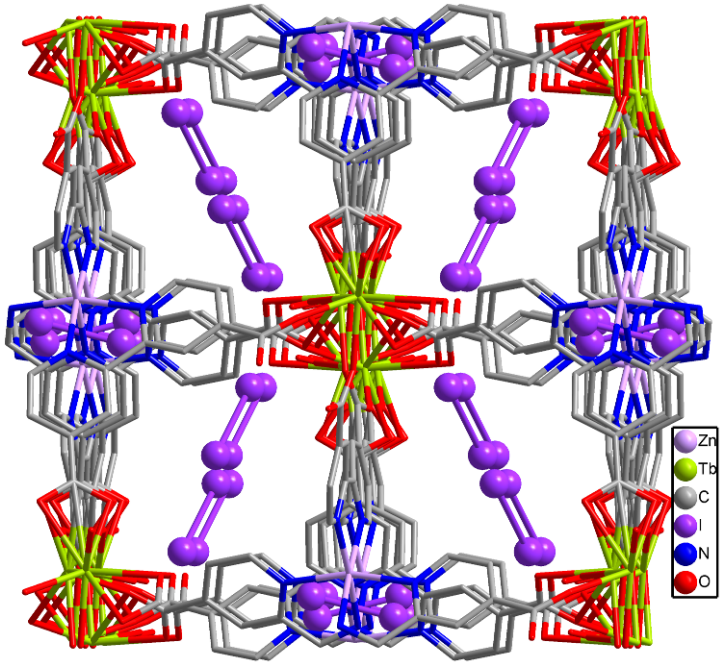

Fig. S1 The 3D framework of **2**·$\mathbf{I^-}$.

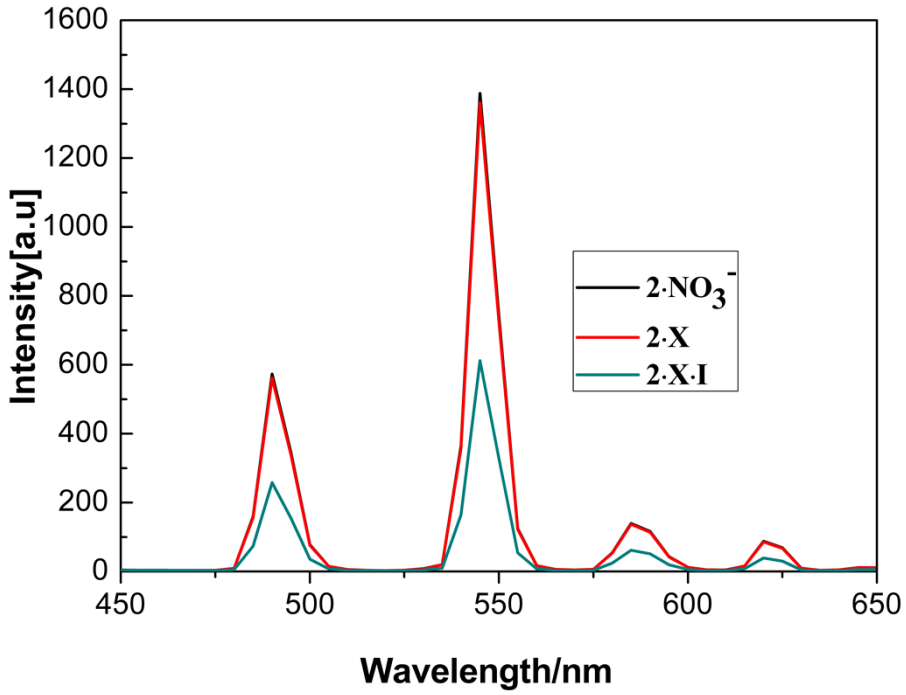

Fig. S2 The liquid PL spectra of **2**·$\mathbf{NO_3^-}$, **2**·**X** and **2**·**X**·$\mathbf{I^-}$ (excited at 343 nm).

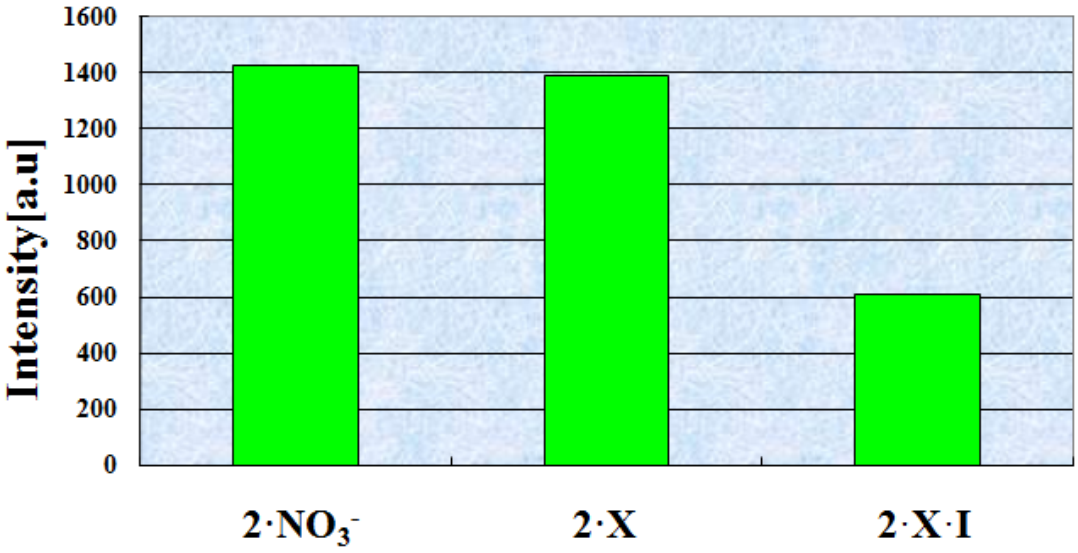

Fig. S3 $^5D_4 \rightarrow {}^7F_5$ transition intensities of **2**·$\mathbf{NO_3^-}$, **2**·**X** and **2**·**X**·$\mathbf{I^-}$ (excited at 343 nm and monitored at 545 nm).

The detection limit was calculated based on the luminescence intensity change *vs* log*C* curve of I^- (1×10^{-8}~1×10^{-4} mol·L^{-1}), shown in Fig. S5. The luminescence intensity of I^- was measured by three times and the standard deviation of blank measurement was achieved. The detection limit was calculated with the following equation: Detection limit = $3\sigma/k$, where σ is the standard deviation of blank measurement, k is the slop between the luminescence intensity versus logC_I.

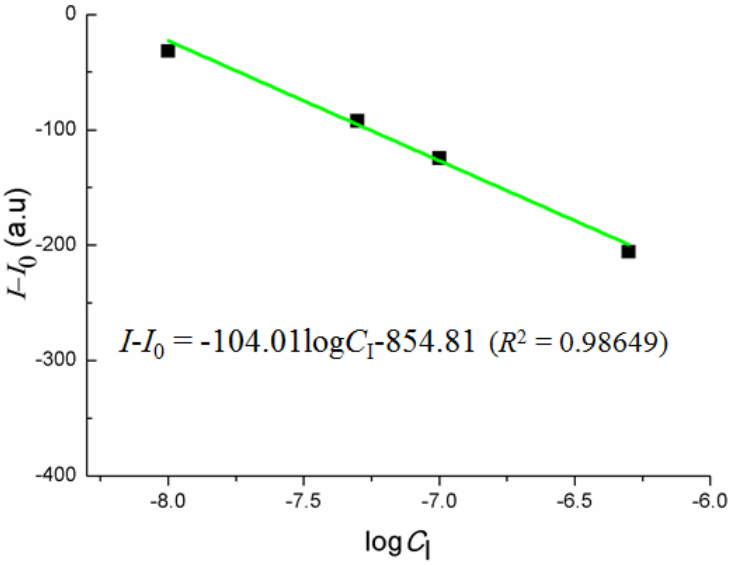

Fig. S4 The fitting of luminescence intensity change (I-I_0) of **2**·NO_3^- *vs* logC_I.

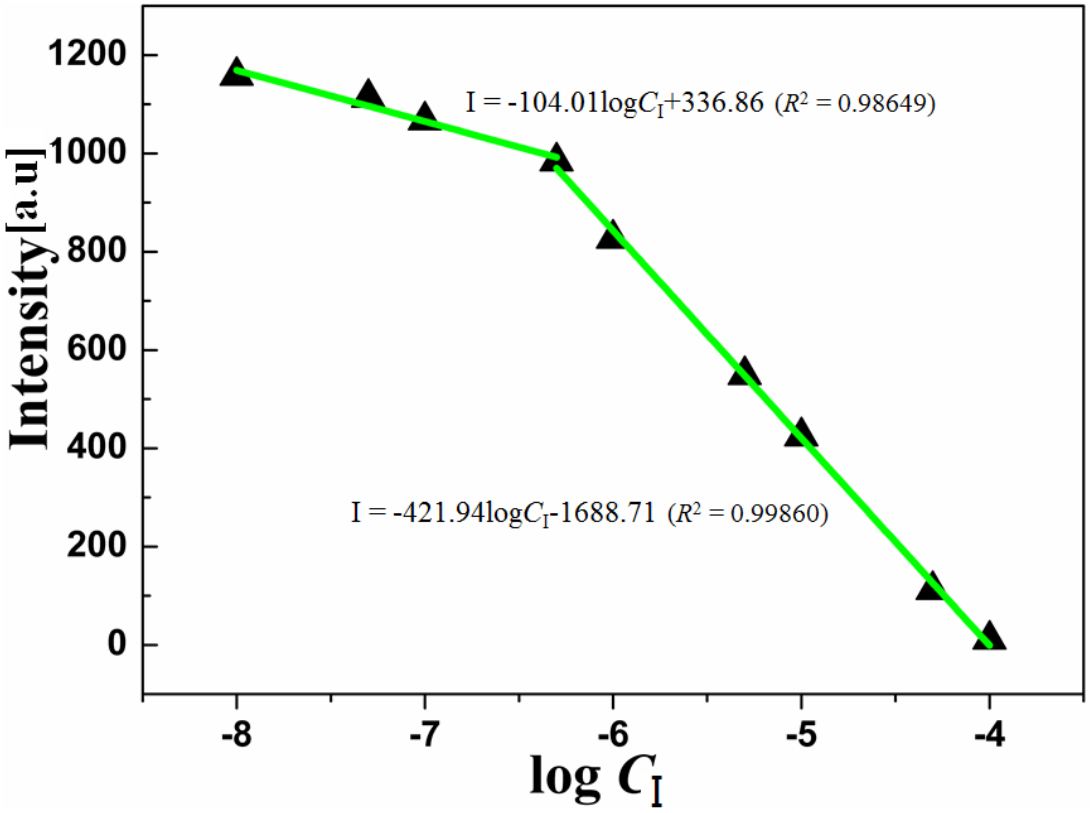

Fig. S5 The intensity plots **of 2**·NO_3^- *vs* logC_I

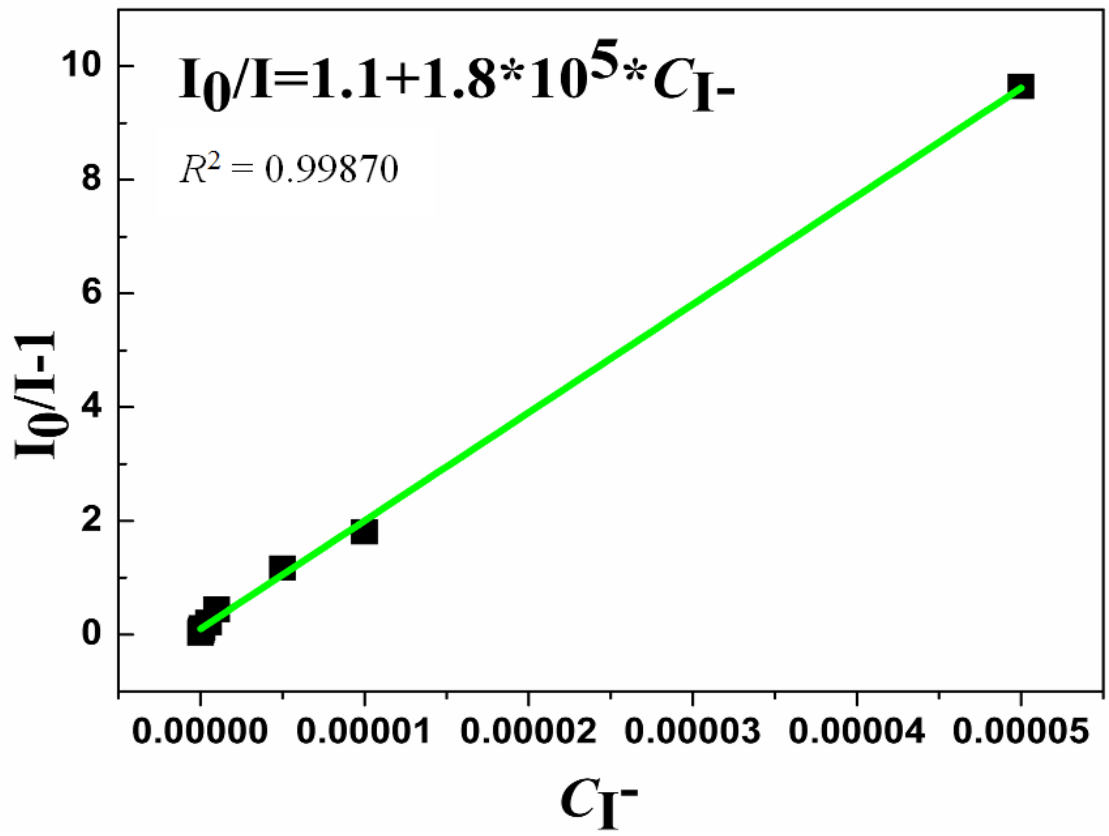

Fig. S6 The Stern-Volmer plot of 2·NO_3^- was quenched by KI aqueous solution.

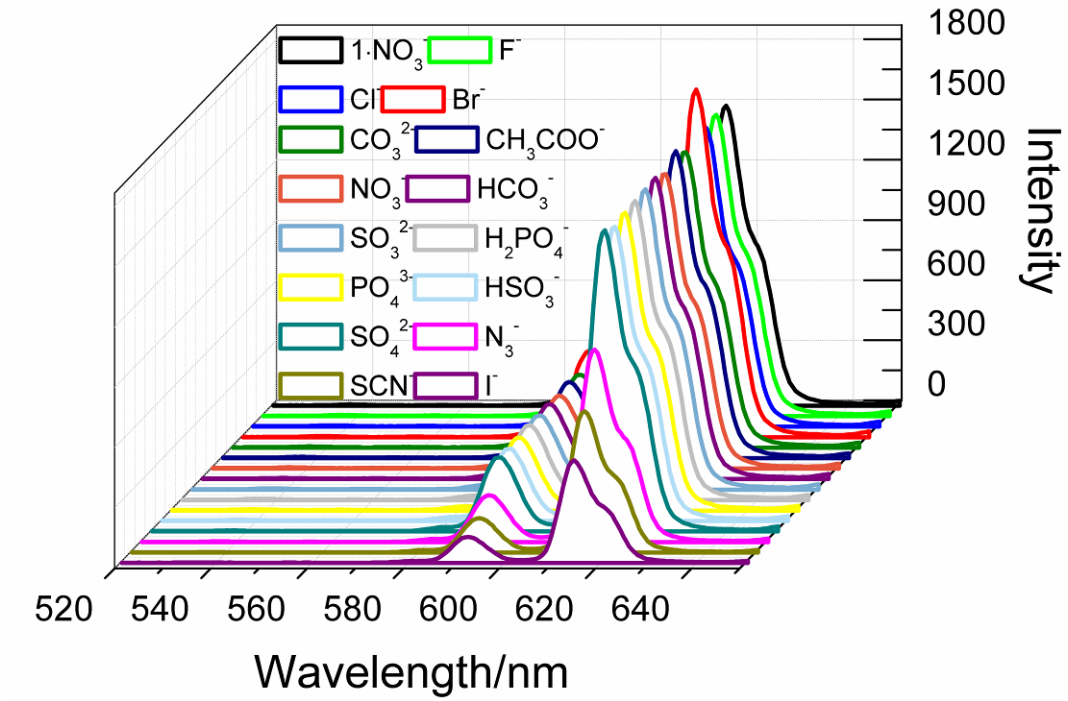

Fig. S7 PL spectra of **1**·NO_3^- after immersed in various anions aqueous solutions (excited at 343 nm).

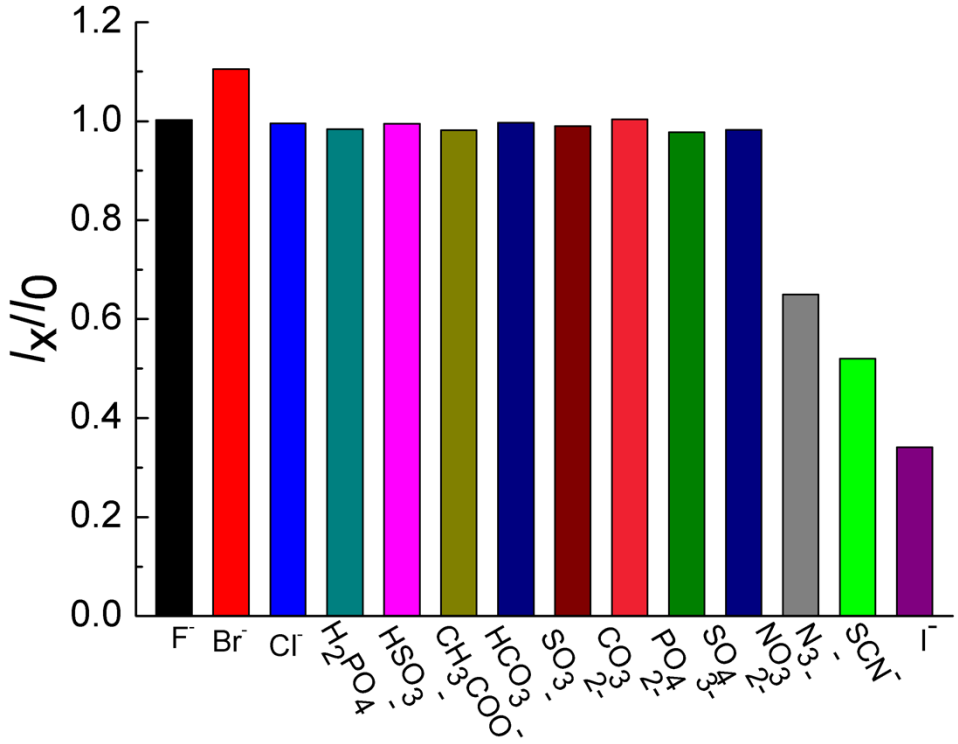

Fig. S8 The ratio of $^5D_0 \rightarrow {}^7F_2$ transition intensities of **1**·$\mathbf{NO_3^-}$ immersed in various 5×10^{-5} mmol K_mX aqueous solutions (I_x) to the **1**·$\mathbf{NO_3^-}$ immersed in distilled water (I_0) (excited at 343 nm and monitored at 615 nm).

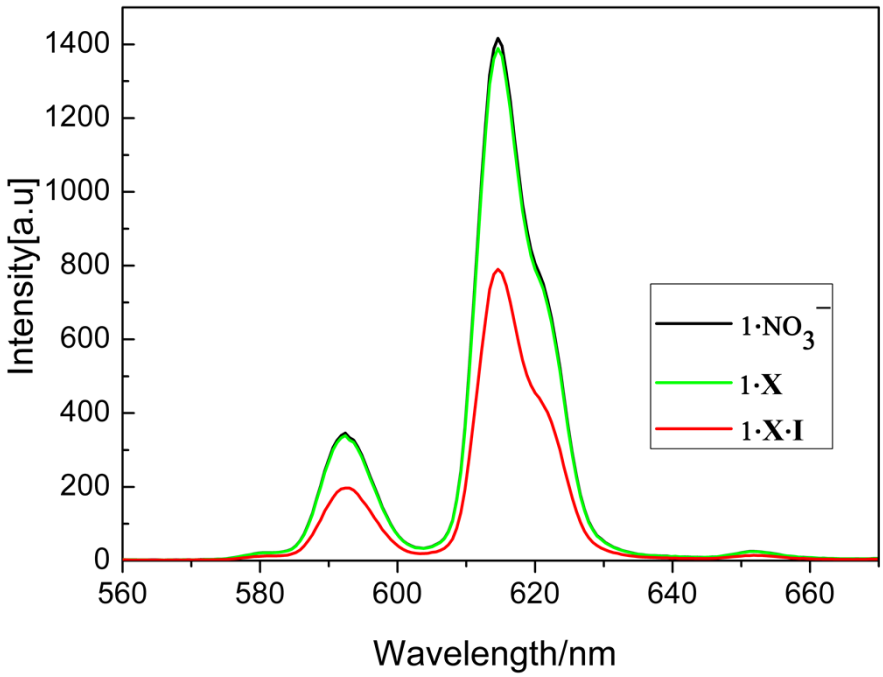

Fig. S9 The liquid PL spectra of **1**·$\mathbf{NO_3^-}$, **1**·**X**, and **1**·**X**·$\mathbf{I^-}$ (excited at 343 nm).

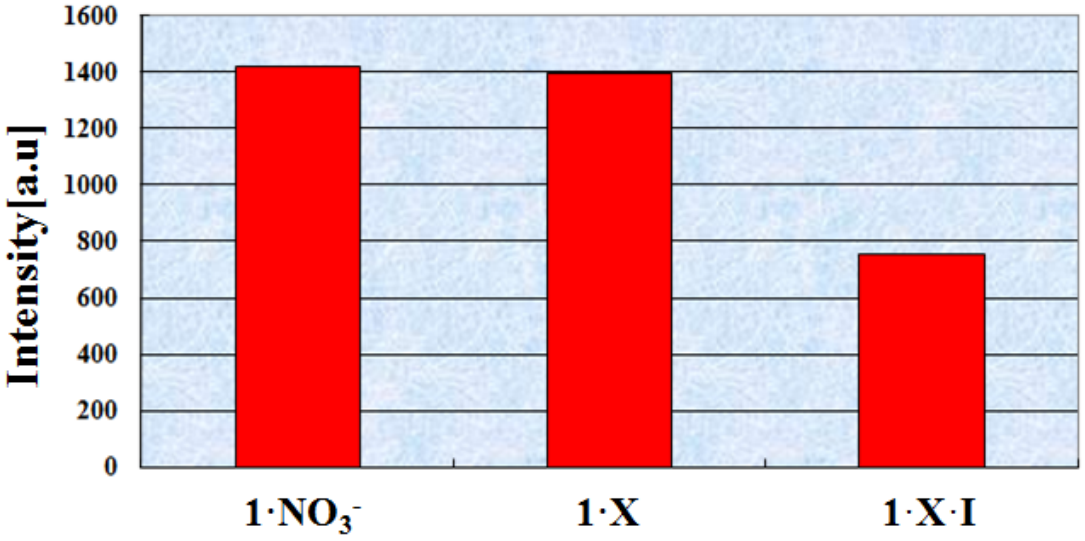

Fig. S10 $^5D_0 \rightarrow {}^7F_2$ transition intensities of **1**·NO_3^-, **1**·**X** and **1**·**X**·I^- (excited at 343 nm and monitored at 615 nm).

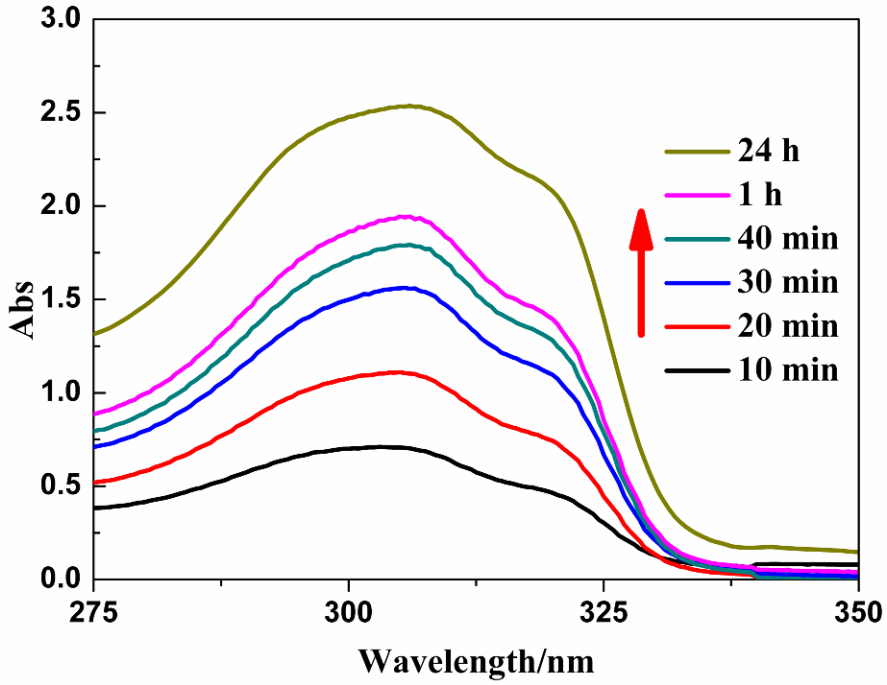

Fig. S11 UV spectra of the KI solution after **1**·NO_3^- was added.

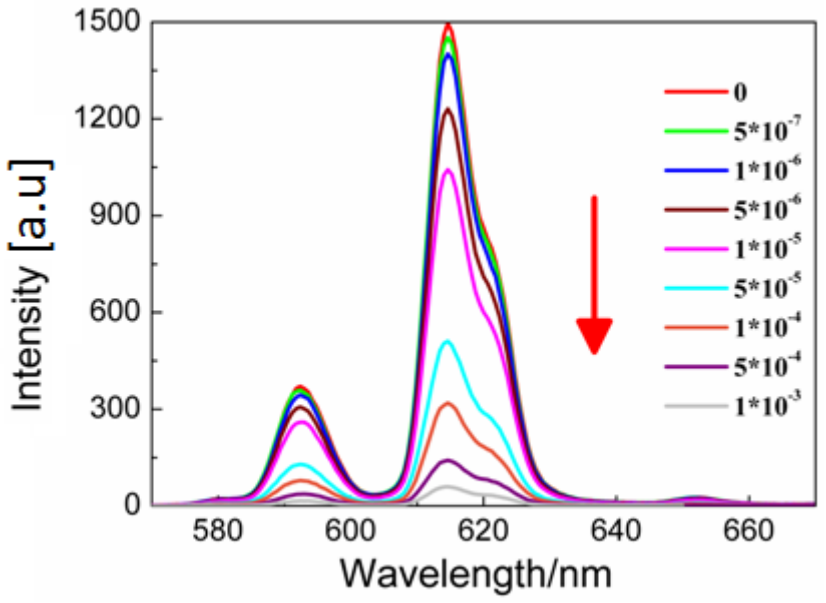

Fig. S12 The liquid PL spectra of **1**·NO_3^- under different concentrations of KI aqueous solution (mol/L) upon excited at 343 nm.

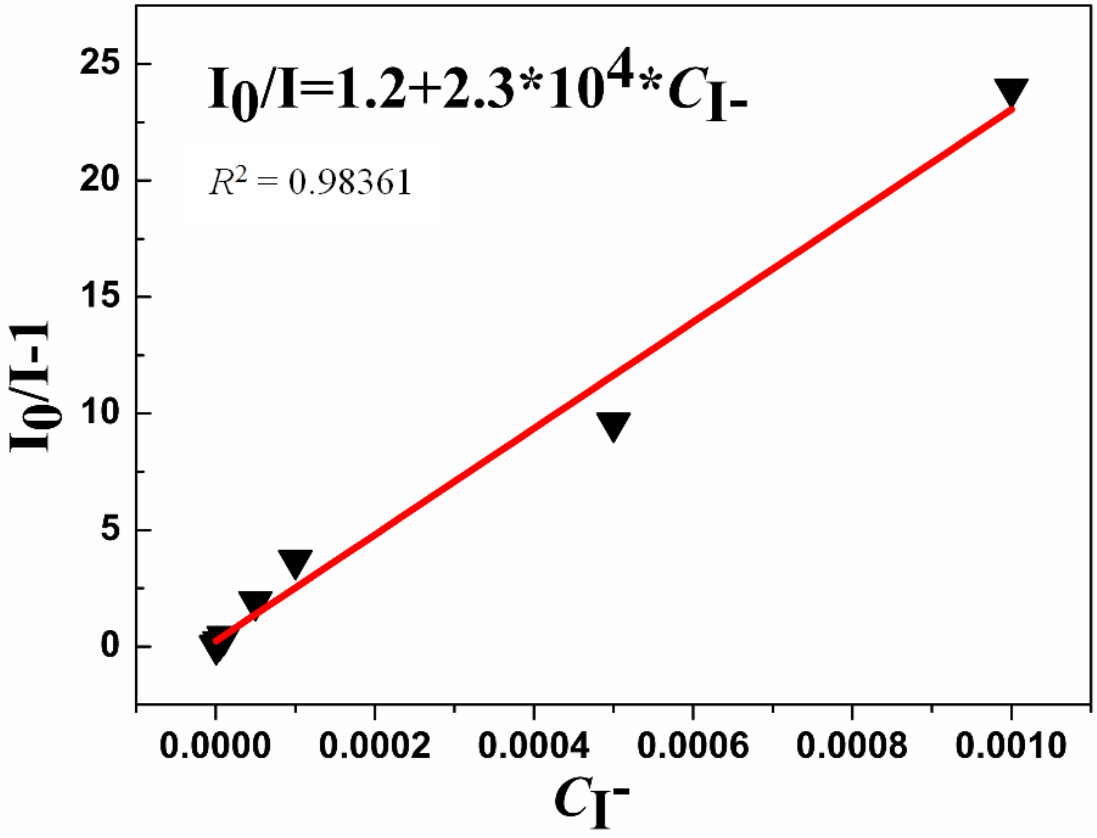

Fig. S13 Stern-Volmer plot of **1**·NO_3^- was quenched by KI aqueous solution.

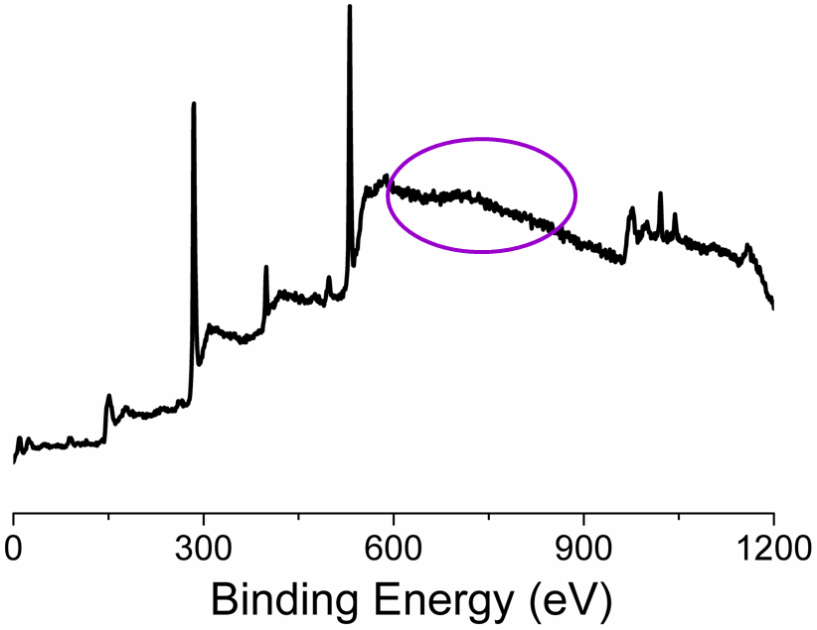

Fig. S14 The XPS spectrum of regenerated **2**·NO_3^- from **2**·I^-.

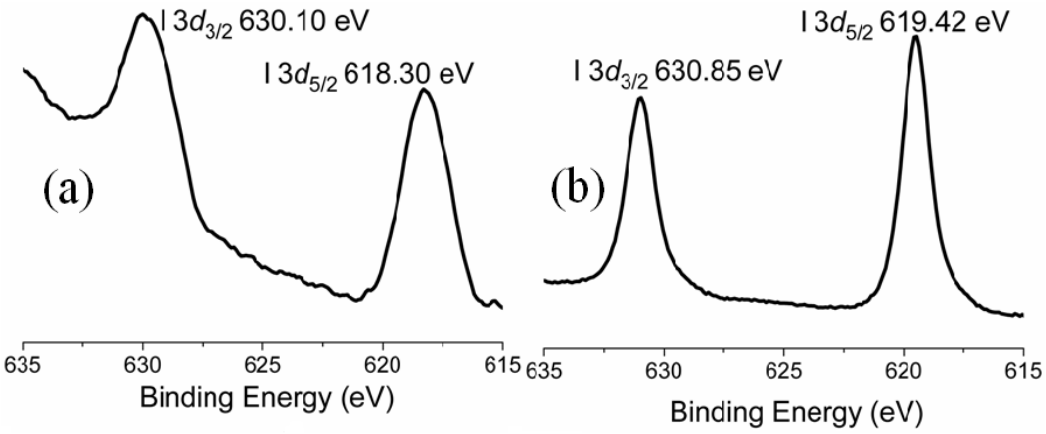

Fig. S15 The XPS spectra of **2**·I^- (a) and AgI (b).

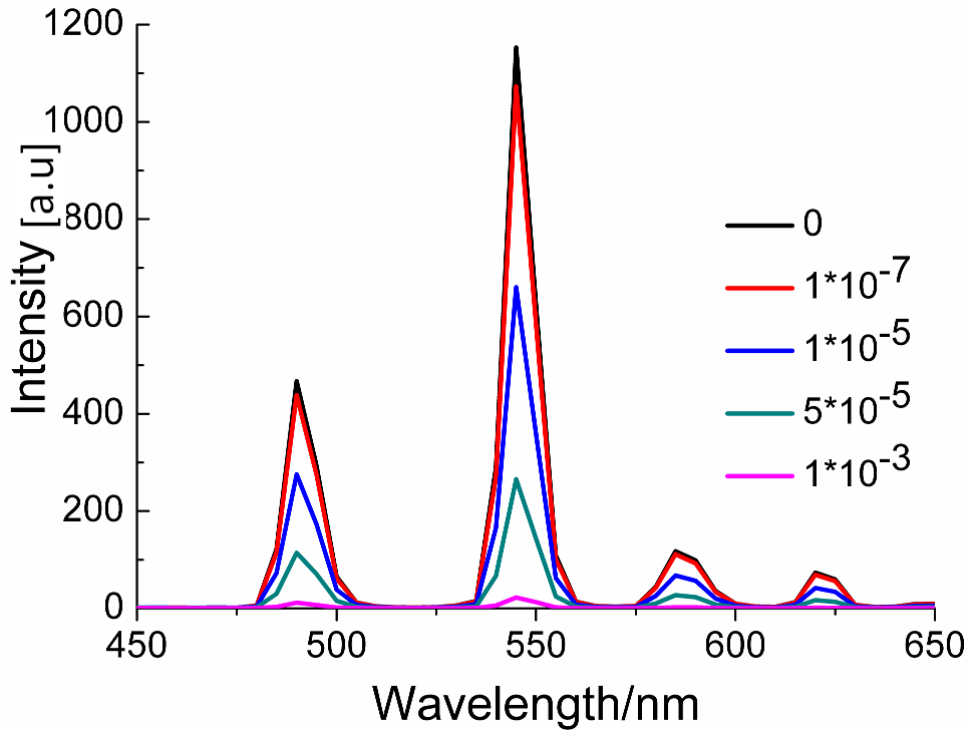

Fig. S16 PL spectra of the regenerated **2**·NO_3^- from the **2**·I^- after 10 cycles under different concentrations of KI aqueous solution (mol/L) upon excited at 343 nm.

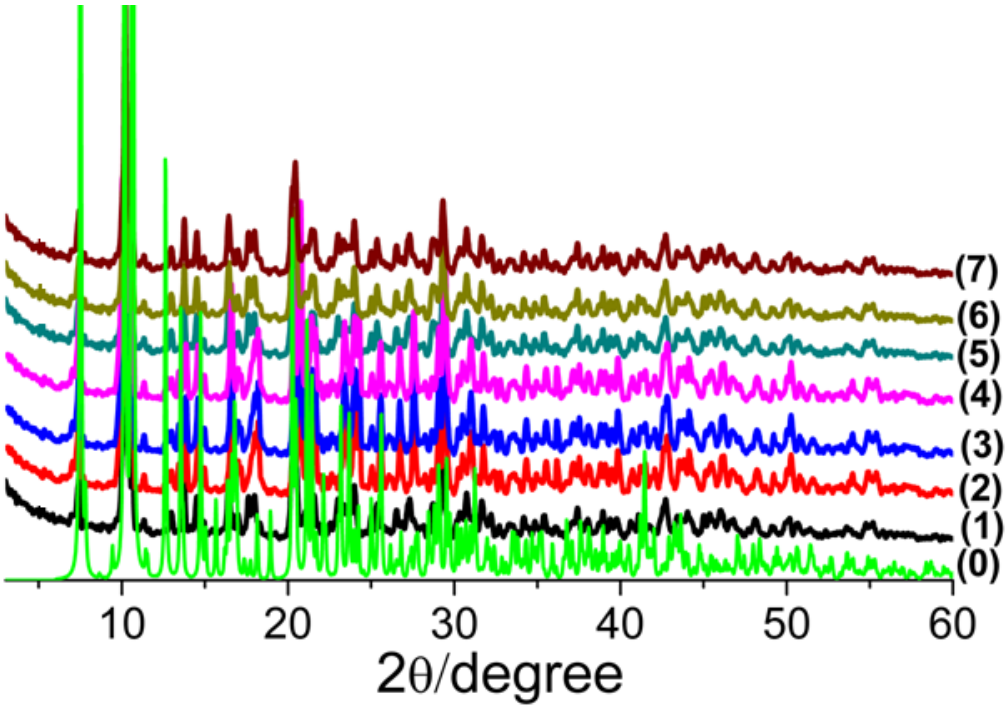

Fig. S17 PXRD patterns of the simulated (0), **1**·NO_3^- (1), **2**·NO_3^- (2), **2**·I^- (3), **1**·I^- (4), regenerated **2**·NO_3^- from **2**·I^- (5), **1**·NO_3^- (6) and **2**·NO_3^- (7) immersed in aqueous for two weeks.

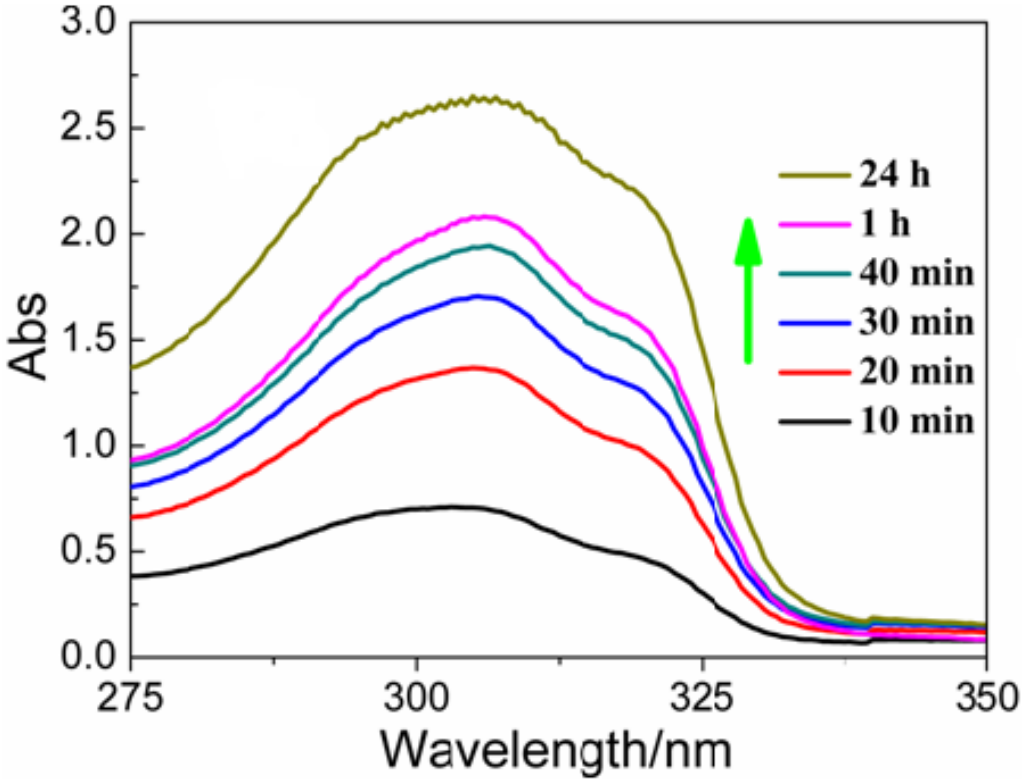

Fig. S18 UV spectra of the KI solution after **2**·NO_3^- was added.

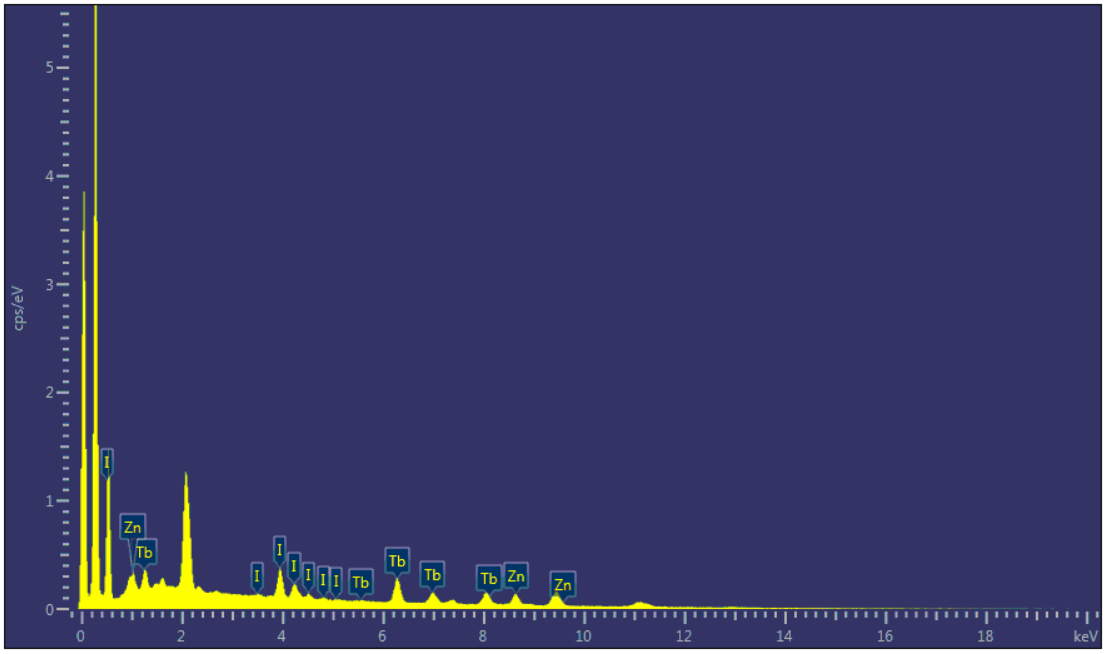

Fig. S19 The EDS mapping of **2**·I^-.

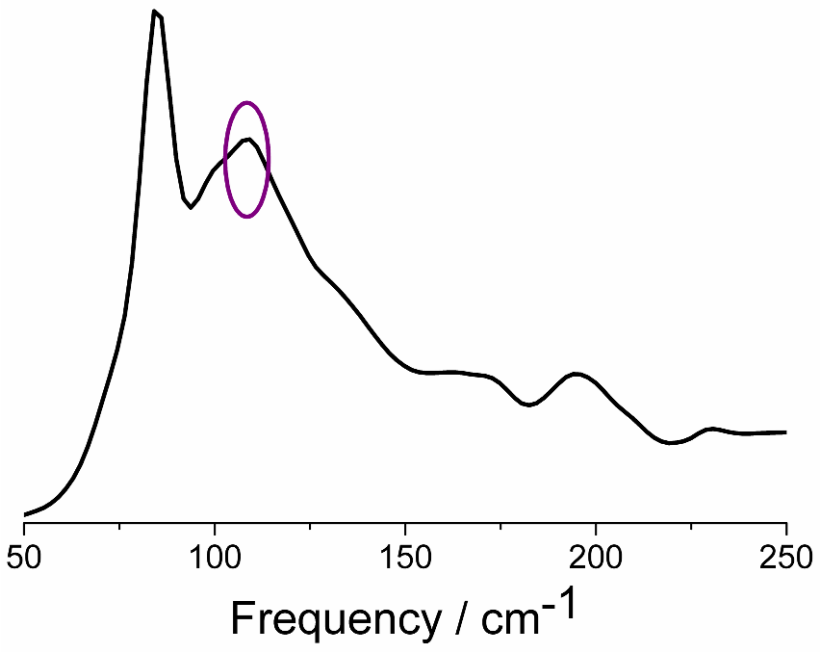

Fig. S20 The Raman spectrum of **2**·$\mathbf{I^-}$.

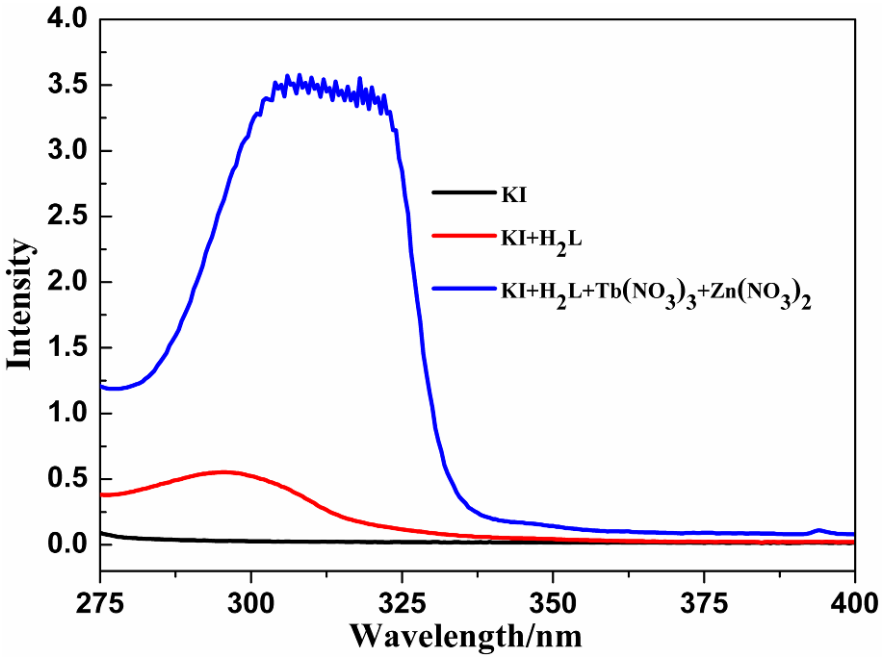

Fig. S21 UV spectra of the solutions: KI, KI+H_2L and KI+H_2L+$Tb(NO_3)_3$+$Zn(NO_3)_2$.

The formation of I_2 was further studied in mionectic environment. **2**·$\mathbf{NO_3^-}$ solid samples and KI solution were placed in vacuum tube with inletting Ar gas respectively, and the gas suction and exhaust were proceeding for 20 minutes. Then, KI solution was introduced into the vacuum tube contained the **2**·$\mathbf{NO_3^-}$ samples by steel needle. After three minutes, weak color change of the solid sample took place from colorless to pale yellow. Simultaneously, the same experiments were carried out,

but in air. Amazingly, the color change from colorless to yellow is very fast within only 1 minute (Fig. S20). Thus, the oxidization of I^- in **2**·$\mathbf{NO_3^-}$ in air is quicker than that in mionectic environment. The results indicate that, just as what you expected, the oxidization of I^- in **2**·$\mathbf{NO_3^-}$ is relevant to the amount of O_2.

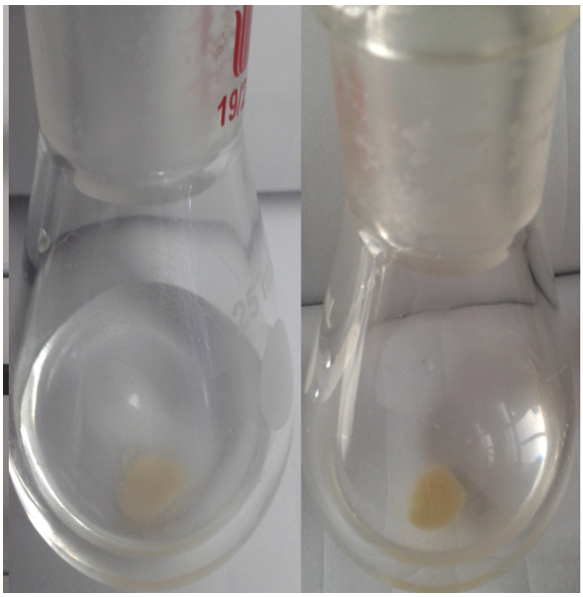

Fig. S22 The **2**·$\mathbf{NO_3^-}$ and KI solution in mionectic enviroment (left) and in air (right).

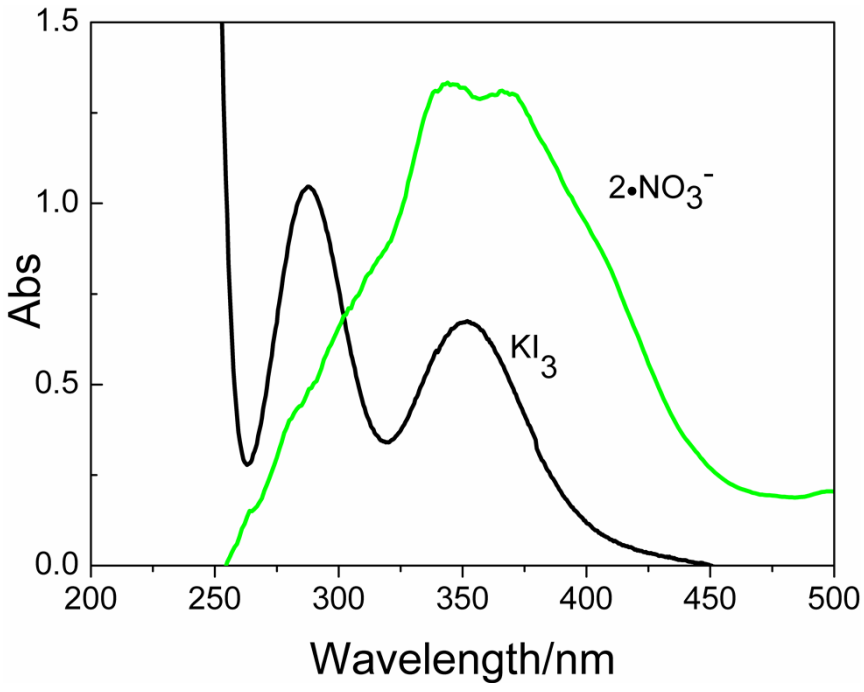

Fig. S23 UV spectra of the KI_3 solution (black line) and the solid samples of **2**·$\mathbf{NO_3^-}$ (green line).

Single crystal structure analyse of the crystal **2-Br**$^-$ (**2-**$\mathbf{NO_3^-}$ after immersed in KBr) also indicates Br^- exchanged with NO_3^- and entered into the channels, although the

crystal data is not perfect. Br^- in the channels and the coordinated water molecules on the Tb or Eu atoms form strong H-bonding with the Br-O distance of 2.74 Å and bond angle Br-H-O of 164.36°. The formation of H-bonding decreases the energy consumption from the O-H vibrations, and indirectly increases the energy transfer from ligand L^{2-} to Eu/Tb center, resulting in luminescence enhancement (Fig. S23). Furthermore, the heavy atom effect of Br^- can enhance the intersystem crossing efficiency from *S*1 to *T*1, (*S*1 and *T*1 represent the excited state and the triplet state, respectively, Fig. S24)[10], and result in the luminescence enhancement. Neither SCN^- nor N_3^- has absorption peaks from 240 to 375 nm in the UV-Vis spectra (Fig. 25, 26), and both of them can weaken the luminescence of **1**·$\mathbf{NO_3^-}$ and **2**·$\mathbf{NO_3^-}$. We also attempt to further explore the mechanism of luminescence response to SCN^- and N_3^-, but the positions of them in channels did not be determined by single-crystal diffraction technology.

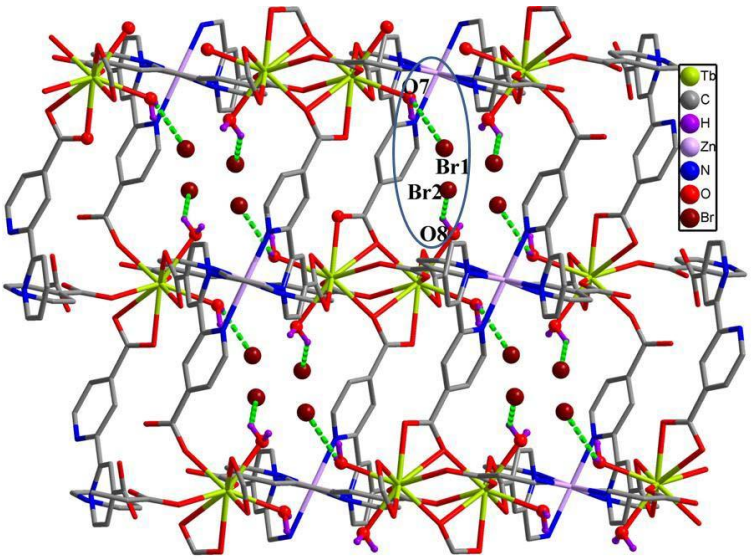

Fig. S24 The H-Bonding (green line) between Br^- and coordination water molecules in crystal **2**-$\mathbf{NO_3^-}$ after immersed in KBr.

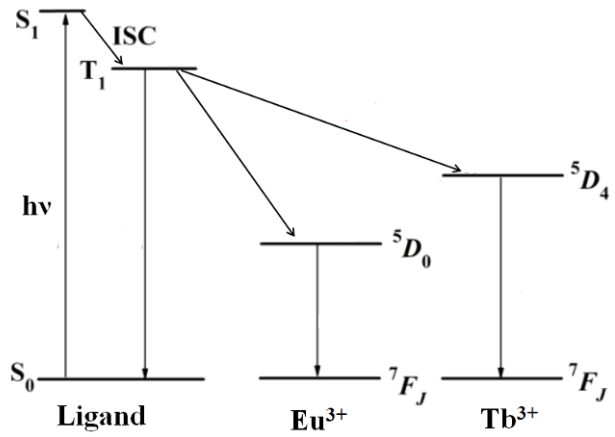

Fig. S25 The energy absorption and emission process in **1**·NO_3^- and **2**·NO_3^-.

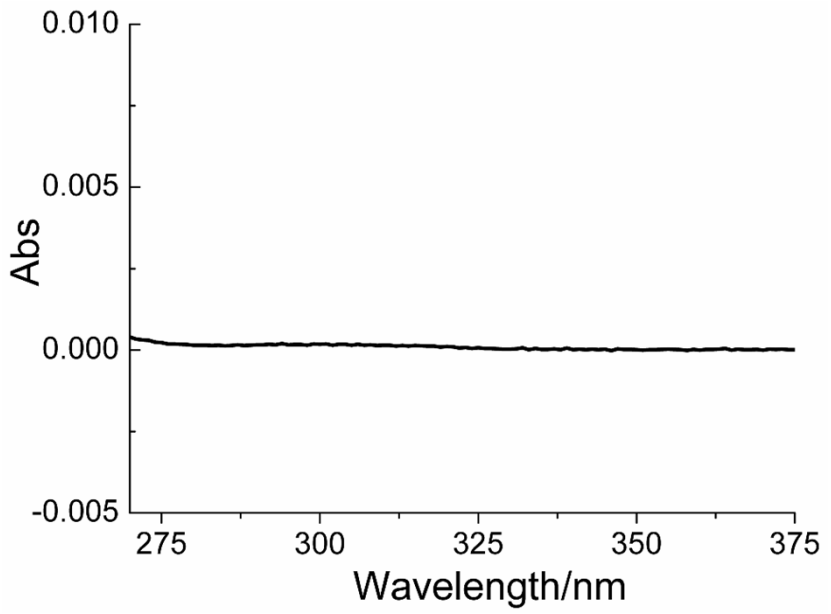

Fig. S26 UV-Vis spectrum of the NaN_3 solution.

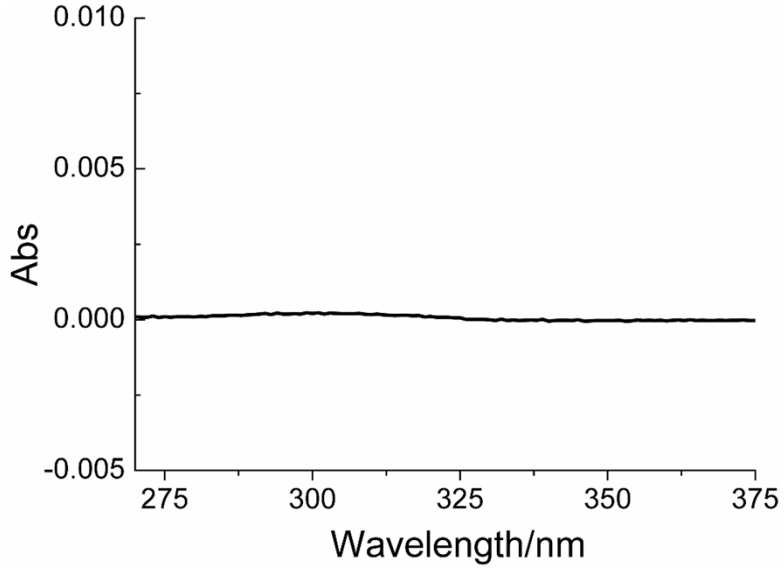

Fig. S27 UV-Vis spectra of the KSCN solution.

Thermogravimetric Analysis（TGA）

The TGA curves of **1**·NO_3^- and **2**·NO_3^- exhibit two steps of weight loss. The first weight loss of 19.31 % for **1**·NO_3^- and 18.46 % for **2**·NO_3^- in the range of 25 °C and 100 °C arise from the loss of free water molecules and coordinated water molecules, which is well consistent with the calculated 19.10 % for **1**·NO_3^- and 18.92 % for **2**·NO_3^-. During the range of 100-360 °C, both of them mainly stay in a plateau, indicating high thermal stability for these two MOFs. The second weight loss above 360 °C stems from the decomposition of 3D frameworks.

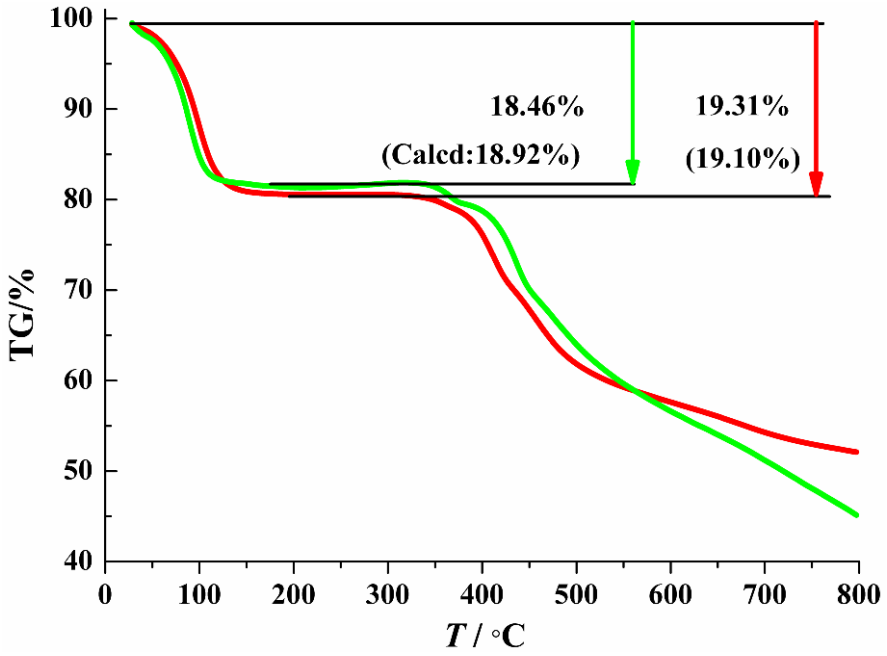

Fig. S28 The TGA curves of **1**·NO_3^- (red line) and **2**·NO_3^- (green line).

Table S1. Response time and lowest detection limit in some MOFs as luminescent Probes

MOF	Detected object	Response time	Detection limits (mol/L)	[Ref]
Eu-MOF	Fe^{3+}	1 min	1×10^{-4}	2
Eu-MOF	Cu^{2+}	--	1×10^{-5}	3
Tb-MOF	PO_4^{3-}	--	1×10^{-4}	4
Eu-MOF	Fe^{3+}	4 h	1×10^{-4}	5
Zn-MOF	Cu^{2+}	--	1×10^{-3}	6
Eu-MOF	DMF	10~20 s	--	7
Zn-MOF	Explosives	10 s	--	8
Ir-MOF	O_2	30 s	--	9
2·NO_3^-	I^-	10 s	1×10^{-8}	in this work
1·NO_3^-	I^-	10 s	5×10^{-7}	in this work

Table S2. Crystal data and structure refinement for 1·NO_3^-, 2·NO_3^-, 2-Br^- and 2·I^-

Complex	**1**·NO_3^-	**2**·NO_3^-	**2**·Br^-	**2**·I^-
Formula	$C_{36}H_{50}Eu_2N_8O_{34}Zn$	$C_{36}H_{50}Tb_2N_8O_{34}Zn$	$C_{72}H_{52}Br_4N_{12}O_{62}Tb_4Zn_2$	$C_{72}H_{52}I_4N_{12}O_{42}Tb_4Zn_2$
Fw	1508.15	1522.07	3163.32	3031.28
Crystal system	Monoclinic	Monoclinic	Monoclinic	Monoclinic
Space group	*C*2/c	*C*2/c	*C*2/c	*C*2/c
a, Å	17.0712(9)	17.0778(7)	17.0516(9)	17.2316(6)
b, Å	16.9810(11)	16.9284(4)	16.9331(10)	16.7585(7)
c, Å	20.3832(10)	20.3385(9)	20.3267(14)	21.2567(7)
α, deg	90.00	90.00	90.00	90.00
ß, deg	108.073(6)	108.115(5)	107.781(7)	106.996(4)
γ , deg	90.00	90.00	90.00	90.00
V, $Å^3$	5617.3(5)	5588.4(4)	5588.7(6)	5870.3(4)

Z	4	4	4	2
Dc, g/cm^3	1.755	1.780	1.880	1.715
F(000)	2904	2920	3048	2872
μ, mm^{-1}	2.731	3.031	4.453	3.908
GOF on F^2	1.048	1.053	1.052	1.034
R_1/wR_2(I>2σ(I))	0.0582/0.1350	0.0523/0.1294	0.0658/0.1606	0.0548/0.1255

References

1. P. H. Svensson and L. Kloo, *Chem. Rev.* 2003, **103**, 1649.
2. M. Zheng, H. Q. Tan, Z. G. Xie, L. G. Zhang, X. B. Jing and Z. C. Sun, *Appl. Mater. Interfaces* 2013, **5**, 1078.
3. B. L. Chen, L. B. Wang, Y. Q. Xiao, F. R. Fronczek, M. Xue, Y. J. Cui and G. D. Qian, *Angew*. *Chem*., *Int*. *Ed*. 2009, **48**, 500.
4. H. Xu, Y. Q. Xiao, X. T. Rao, Z. S. Dou, W. F. Li, Y. J. Cui, Z. Y. Wang and G. D. Qian, *J. Alloys*. *Compd*. 2011, **509**, 2552.
5. S. Dang, E. Ma, Z.M. Sun and H. J. Zhang, *J. Mater*. *Chem*. 2012, **22**, 16920.
6. S. Liu, Z. H. Xiang, Z. Hu, X. P. Zheng and D. P. Cao, *J. Mater. Chem.* 2011, **21**, 6649.
7. Y. Li, S. S. Zhang and D. T. Song, *Angew*. *Chem*., *Int*. *Ed*. 2013, **52**, 710.
8. A. J. Lan, K. H. Li, H. H. Wu, D. H. Olson, E. J. Emge, W. Ki, M. C. Hong and J. Li, *Angew*. *Chem*., *Int*. *Ed*. 2009, **48**, 2334.
9. Z. Xie, L. Ma, K. E. deKrafft, A. Jin and W. Lin, *J*. *Am*. *Chem*. *Soc*. 2010, **132**, 922.
10. J. C. Koziar and D. O. Cowan, *Acc*. *Chem*. *Res*. **1978**, 334.